PHYSICAL REVIEW E **88**, 030201(R) (2013)

Drag on intruders in granular beds: A boundary layer approach

Jonathan Goldsmith,[1] Hong Guo,[2,3] Shelby N. Hunt,[1] Mingjiang Tao,[3] and Stephan Koehler[1,*]

[1]*Department of Physics, Worcester Polytechnic Institute, Worcester, Massachusetts 01609, USA*

[2]*College of Water Resources and Architectural Engineering, Northwest A&F University, Yangling 712100, People's Republic of China*

[3]*Department of Civil and Environmental Engineering, Worcester Polytechnic Institute, Worcester, Massachusetts 01609, USA*

(Received 3 October 2012; revised manuscript received 2 August 2013; published 30 September 2013)

We performed a parametric study of the drag on vertical intruders with uniform cross sections of different sizes and shapes, from which we developed a semiempirical model. Baffling techniques were used to isolate the contributions of the intruder's different subsurfaces, and we observed size effects and force focusing on edges. We propose a boundary layer approach, whereby the drag is the surface integral of an effective stress over a monolayer of particles contacting the intruder. The stress has a simple lithostatic dependence and is a function of the orientation relative to the intruder's direction of motion. This approach is experimentally verified and is consistent with the semiempirical model.

DOI: 10.1103/PhysRevE.88.030201 PACS number(s): 45.70.Mg, 47.57.Gc, 61.43.−j

Most of the Earth's surface is covered with granular matter: sand in deserts, soil in fertile regions, snow in cold climates, and sediments underneath bodies of water. Consequently many industrial, geotechnical, and agricultural processes involve granular materials [1,2]. Examples are mixing, plowing, and excavation which involve moving boundaries (i.e., intruders) that interact with the granular material. Previous studies of intruder drag in dense granular media (DGM) were performed by Schiffer *et al.* [3,4] who used a bluff-body approach for partially immersed posts. More recently Goldman's group used resistive force theory for the drag on fully immersed slender intruders [5]. Both of these continuum approaches successfully captured many experimental features. However several issues remain unresolved, which include effects of the particle size, the intruder's cross-sectional shape on the drag, and force focusing on intruder edges. Here we address these issues by performing systematic drag experiments and developing a continuum boundary layer approach that also incorporates granular size effects.

Flowing granular media and fluids have many features in common, such as pattern formation, longitudinal vortices, and long surface waves [2]. Resistive force theory developed for slender bodies in viscous fluids has been adapted to slender intruders moving through granular beds [5]. Other similarities involve boundary layers, which occur at surfaces of granular and laminar flows [6]. In aerodynamics boundary layers surround moving intruders and increase the drag [7]. Likewise in DGM, intruders experience increasing drag with particle size [8,9], which we show can be modeled as a boundary layer effect where the thickness scales with particle size.

Two types of continuum approaches for drag on intruders partially immersed in DGM have been developed. One is based upon classical Coulomb treatment of soils, whereby the motion of a semi-infinite plate results in a two-dimensional shear band wedge extending from the intruder bottom to the free surface. This approach has recently been adapted for drag on wide plates [10,11], but is inadequate for slender intruders, such as posts where the flow is three dimensional. Another approach resembles bluff-body drag [3]. The drag force is proportional to the integral over the intruder's area projected along its advancing direction of the lithostatic pressure

$$p \propto \rho g z, \tag{1}$$

where ρ, g, and z are the bulk density, gravitational acceleration, and depth below the free surface, respectively. Neither approach accounts for the cross-sectional shape, nor is the scale effect considered. In the case of large particles the latter can be substantial.

Drag experiments were performed by partially immersing intruders in a granular flow, similar to placing airfoils in wind tunnels. A large square granular bed, of dimensions $70 \times 60 \times 9$ cm, is mounted on an xy translation stage that is actuated by stepper motors. It is filled with glass beads having diameter $d = 5 \pm 0.5$ mm, and material density 2.55 g/cm^3. The beads are prepared in the critical state [12] by raking the bed twice and leveling. The packing fraction is 60%, which remains constant throughout the experiment [13] giving a bulk density of $\rho = 1.53$ g/cm^3. The dragging speed is sufficiently slow, $v = 1$ cm/s, such that inertial effects are negligible and sliding friction is dominant. The intruders' shapes are square bars and cylindrical posts, all with uniform cross sections and flat bottoms. The forces are measured by mounting the immersed intruders onto load cells, and we report the steady-state forces averaged over 10 cm of travel.

Figure 1 shows the drag for square bars and posts over a range of widths and diameters, W, and immersion depths, $Z = 0.5, 1, 2, \ldots, 7$ cm. For wide intruders, $W > \{Z, d\}$, the drag force increases supralinearly (almost quadratically) with the intruder's width; however, the bluff-body approach predicts a linear increase because the projected area scales linearly with width. For narrow intruders, $W < d$, the drag approaches a nonzero value; however for this limit the bluff-body approach predicts zero drag. These experiments indicate the need for a more robust model that also accounts for particle size.

We seek a functional form for the drag force using dimensional analysis. Rescaling the drag force by ρg gives a volume, and a Taylor expansion results in linear combinations of the following terms: $WZ^2, W^2Z, Z^2d, WZd, \cancel{W^2d}, \cancel{Wd^2}, \ldots$. The last two terms can be eliminated because the drag force cannot be independent of immersion depth and we neglect

*Present address: Department of Physics, Harvard University, Cambridge Massachusetts 02138, USA; koehler@seas.harvard.edu

 ©2013 American Physical Society

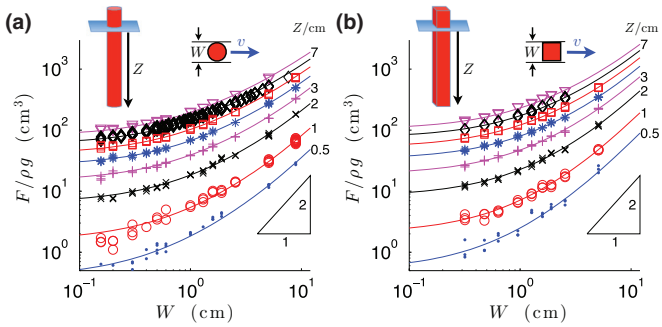

FIG. 1. (Color online) Drag force dependence on width at different immersion depths Z for (a) posts and (b) square bars in $d = 5$ mm beads. Curves from Eq. (2) using parameters from Table I.

higher-order terms involving the particle size such as d^2,d^3. This leaves for the drag dependence

$$\frac{F}{\rho g} = c_s W Z^2 + c_b W^2 Z + k_s Z^2 d + k_b W Z d. \qquad (2)$$

The curves in Fig. 1 are in good experimental agreement for a large range of intruder dimensions. The fitting coefficients are listed in Table I and exhibit some shape dependence (square vs circe). The Supplemental Material [14] includes a sensitivity analysis showing how each of the four terms contributes over parameter space. Hence Eq. (2) is a minimal semiempirical model that describes our measurements.

The terms of Eq. (2) are integrals of the scaled pressure, Eq. (1), over immersed surfaces: $\int z\, dA$. The first term, $c_s W Z^2$, is due to side faces. It dominates for deep immersions and captures Schiffer's bluff-body approach. Moreover the coefficient c_s for circle and square intruders is almost the same, as would be expected from a bluff-body approach. The second term, $c_b W^2 Z$, is due to drag on the bottom face. The third term represents an integral of the scaled stress along a side edge multiplied by the smallest dimension, which is a particle diameter: $d \int z\, dz$. (Later we discuss the meaning of the term $k_s Z^2 d$ for posts as these do not literally have side edges.) The last term represents an integral of the rescaled stress along the bottom edge multiplied by the particle diameter.

The edge force terms are similar to intruder augmentation as discussed in Chehata's hopper study [8] and Soller's rotating vane study [9]. According to the first term of Eq. (2), augmenting the side width by αd (i.e., $W \to W' = W + \alpha d$) increases the drag by $\alpha c_s \rho g Z^2 d$. The ratio $\alpha = k_s/c_s$ is in the range of 1.5–2, which is close to the amount of side augmentation reported for vanes. Augmentation at the bottom of an intruder face by αd (i.e., $Z \to Z' = Z + \alpha d$) increases the drag by $2\alpha c_s \rho g Z d$, which is reflected in the ratio of the terms $1 < k_b/c_s = 2\alpha < 2$. The parametric study confirms that the effective intruder dimensions are increased

TABLE I. Fitting coefficients to Eq. (2) for both shapes.

	c_s	c_b	k_s	k_b
Circle	2.1 ± 0.1	0.5 ± 0.1	3.3 ± 0.1	2.9 ± 1.2
Square	2.2 ± 0.2	1.0 ± 0.2	4.2 ± 0.3	3.8 ± 2.4

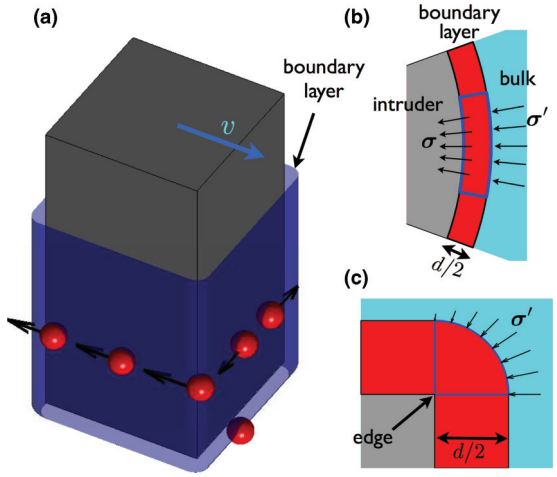

FIG. 2. (Color online) (a) Schematic of a moving square bar and its surrounding boundary layer. Flows of representative particles contacting the intruder in the middle region and the bottom edge are shown. Plane views of the boundary layers surrounding (b) a post and (c) the corner of a square bar.

by about one particle diameter on the sides and the bottom. This observation naturally led us to the development of the boundary layer approach, which we detail below.

Figure 2(a) schematically shows a boundary layer composed of a monolayer of particles that surrounds the intruder and augments its size. The centers of these particles define the extent of the boundary layer (i.e., the boundary layer thickness is $d/2$). Applying a force balance on the closed curved region in Fig. 2(b), the stresses on the boundary layer $\boldsymbol{\sigma}'$ and on the intruder $\boldsymbol{\sigma}$ obey the relationship

$$R\boldsymbol{\sigma} = (R + d/2)\,\boldsymbol{\sigma}', \qquad (3)$$

where R is the radius of curvature. In the limit $R \to \infty$ the intruder surface is flat and $\boldsymbol{\sigma} = \boldsymbol{\sigma}'$. The limit $R \to 0$ corresponds to an edge [see Fig. 2(c)], which has force distribution

$$\frac{d\mathbf{F}}{dz} = \int \boldsymbol{\sigma}'\, ds' = \frac{d}{2} \int_{\phi}^{\phi+\Phi} \boldsymbol{\sigma}'\, d\phi', \qquad (4)$$

where the last term is an azimuthal integral and Φ is the corner angle (e.g., here $\Phi = \pi/2$).

We next discuss how baffling techniques are used to experimentally determine the force distribution along the intruder's surfaces. This involves attaching the load cell only to a portion of the intruder which is mechanically decoupled from the rest of the intruder, which we call the baffle. Figure 3(a) shows such a configuration for determining forces on a side face portion of a square bar, which has width w. There is a gap between the instrumented portion and the baffle, which is less than 1 mm wide, and thus beads are prevented from entering into the gap.

Figure 3(b) shows the azimuthal dependence of the force components normalized by the lithostatic force, $\rho g \int z\, dA = \rho g w Z^2/2$, giving average dimensionless normal and tangential stress components $\tilde{\sigma}_n$ and $\tilde{\sigma}_t$. These collapse for three different combinations of widths and immersion depths. The solid curves are the best fit of the data to a fifth-order cosine (sine) series for the normal (tangential) components [15]. This

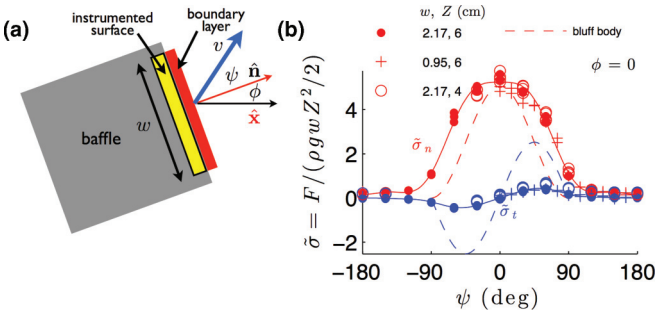

FIG. 3. (Color online) (a) Schematic of intruder baffling with the boundary layer in contact with the instrumented face. The azimuthal angle of the surface normal $\hat{\mathbf{n}}$ is ϕ, and the angle between the surface normal and direction of motion is ψ. (b) Azimuthal dependence of dimensionless components of the normal (red) and tangential (blue) drag forces on side faces (for $\phi = 0$) for three combinations of immersion depth and width: $[w,Z]/\text{cm} = [2.17,6],[0.95,6],[2.17,4]$. Solid curves are Fourier series fitting. Dashed curves show the best fit using the bluff-body drag approach.

leads us to propose a simple form for the stress vector on the boundary layer, $\boldsymbol{\sigma}'$, which is a function of the immersion depth, z, the surface's azimuthal orientation, ϕ, and the orientation of the intruder's motion relative to the surface, ψ [cf. Fig. 3(a)]. Accordingly $\boldsymbol{\sigma}'$ separates into a lithostatic term, a rotation matrix, and dimensionless stress components:

$$\boldsymbol{\sigma}' = \rho g z \begin{pmatrix} \cos(\phi) & -\sin(\phi) \\ \sin(\phi) & \cos(\phi) \end{pmatrix} \begin{pmatrix} \tilde{\sigma}'_n(\psi) \\ \tilde{\sigma}'_t(\psi) \end{pmatrix}. \tag{5}$$

It is informative to explore the applicability of the bluff-body drag approach [3] for the force distribution on intruders. The dashed curves in Fig. 3(b) are the best possible fit, and the poor agreement with experiment indicates this approach is unsuitable for flat surfaces that are not orthogonal to the flow.

In the following experiments we verified the boundary layer approach using the stress dependence, Eq. (5), obtained from fitting the flat surfaces in Fig. 3. Specifically we address the azimuthal dependence of the stress, force focusing on edges and augmentation on curved surfaces.

The inset to Fig. 4(a) highlights a schematic of the instrumented surface, which is the bottom corner of a square intruder. The vertical extent of the contacting boundary layer surface is the augmented height $h' = h + d/2$. The appropriate normalization factor for the corner, $\rho g w h' Z$, gives the dimensionless stresses $\tilde{\sigma}'_n$ and $\tilde{\sigma}'_t$ in Eq. (5) (here $\phi = 0$). Indeed, this normalization collapses the data points for both immersion depths, which also overlay the solid curves that are the fitted dimensionless stress taken directly from Fig. 3(b).

The next verification of the boundary layer approach is for side corners, shown by the inset to Fig. 4(b), which are composed of an edge and two adjacent vertical strips with width w. The predicted drag, colored curves, has contributions from the edge and strips, which are given by Eqs. (4) and (5). This is in good agreement with the measured force components along the corner's center line and tangent, F_x and F_y. For comparison, the gray curves in the background show the forces determined solely from the strips, which fall short of the experimental measurements and indicate the importance of edge forces.

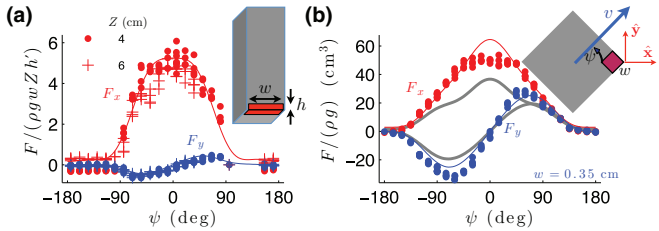

FIG. 4. (Color online) Azimuthal dependence of normal and tangential drag on corners of square intruders. (a) Dimensionless drag on bottom corner, effective width $w = 3.71$ cm and height $h = 0.22$ cm at immersion depths $Z = 4,6$ cm. Height of the integration surface of the stress from the boundary layer approach is $h' = h + d/2$. Curves are the dimensionless stresses from Fig. 3(b). (b) Drag on the side corner, effective width $w = 3.5$ mm. Colored curves in foreground are predictions using the boundary layer approach. Gray curves in the background show the predicted force where the edge contribution has not been included. The inset is a top view showing the corner in red and its orientation.

In Figs. 5(a) and 5(b) we verify the boundary layer approach for posts. The insets show two baffling scenarios where the instrumented regions are a wedge and a semicircle. Following Eq. (5) we normalize the drag force by $\rho g R \Theta Z^2/2$, where $R = W'/2 = (W + d)/2$ is the augmented radius, to obtain the averaged dimensionless stress on the boundary layer over the instrumented region, $\langle \boldsymbol{\sigma} \rangle = \int_\Theta \boldsymbol{\sigma}' \, d\phi/\Theta$. Both figures show that the data collapses for this normalization, and demonstrate good agreement with the boundary layer approach. Figure 5(b) also demonstrates the importance of augmentation: Using $R = W/2$ (i.e., no augmentation) for the small post gives normalized measurements roughly twice their predicted counterparts—see the gray filled circles in the background (for clarity only, the normalized component F_x is shown). Additionally, we verify the boundary layer approach for a new geometry, which is an isosceles triangle intruder immersed to four different depths (see Supplemental Material [14]).

The boundary layer approach accounts for particle size effects for both polygonal and rounded intruders in terms of augmenting the intruder's dimensions. In particular, for an intruder with a convex polygonal shape, the sum of the interior angles is 2π. Consider, for example, the square bar and its

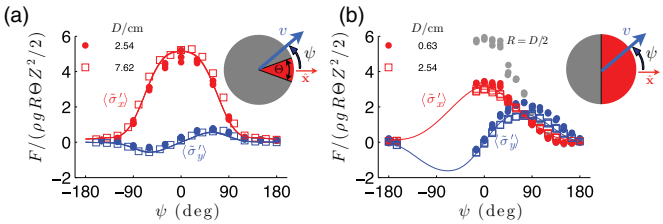

FIG. 5. (Color online) Azimuthal dependence of the averaged, normalized drag forces $\langle \tilde{\boldsymbol{\sigma}}' \rangle$ for regions of posts immersed to $Z = 6$ cm. The colored markers indicate normalization using the augmented radius $R = (W + d)/2$. (a) Wedges from posts with diameters $W = 2.54,7.62$ cm and solid angles $\Theta = 39°,44°$, respectively. (b) Two half-cylinders with diameters $W = 0.63,2.54$ cm. The gray markers are normalized F_x for the smaller half-cylinder using $R = W/2$.

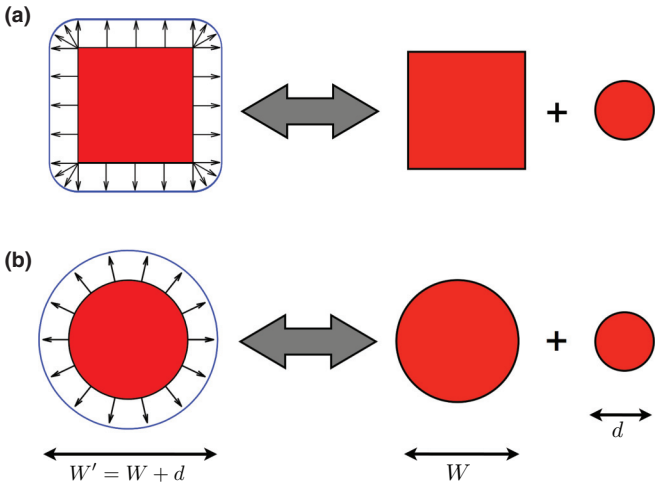

FIG. 6. (Color online) Schematic showing the cross section of the decomposition of the stress on the augmented surface for (a) square bar and (b) cylinder into two contributions, which are the stress on the intruder's surface of width W and a cylinder's surface of diameter d.

surrounding boundary layer shown in Fig. 2(c). The boundary layer regions associated with each of the four sharp corners are wedges that all together form a complete circle. Thus the contribution of the edges to the drag force is equivalent to that of an infinitely thin post, whose augmented diameter is d, immersed to the same depth in a continuum with zero particle size [see Fig. 6(a)]. Likewise for a rounded intruder the amount of augmentation is equivalent to an infinitely thin post immersed at the same depth [see Fig. 6(b)].

We have performed a parametric study of intruder drag and developed a semiempirical model based on dimensional analysis. We use a boundary-layer approach to explain all observed size effects through intruder augmentation and the force balance on the boundary layer. We verify this approach for drag on intruders of various shapes and sizes and on different subsurfaces. The semiempirical model can be reconciled with the proposed boundary layer approach (see the Supplemental Material [14] for details). The boundary layer approach provides a bridge between bulk flow that is treated as a continuum, and force distributions on intruder surfaces that are influenced by the particle size. We believe that this approach may be relevant for other particulate systems, such as colloidal suspensions and slurries.

S.A.K. acknowledges support from NSF CTS 0626191.

[1] P. G. de Gennes, Rev. Mod. Phys. **71**, S374 (1999).
[2] I. S. Aranson and L. S. Tsimring, Rev. Mod. Phys. **78**, 641 (2006).
[3] R. Albert, M. A. Pfeifer, A. L. Barabasi, and P. Schiffer, Phys. Rev. Lett. **82**, 205 (1999).
[4] I. Albert, J. G. Sample, A. J. Morss, S. Rajagopalan, A. L. Barabasi, and P. Schiffer, Phys. Rev. E **64**, 061303 (2001).
[5] R. D. Maladen, Y. Ding, C. Li, and D. I. Goldman, Science **325**, 314 (2009).
[6] K. M. Hill, G. Gioia, and V. V. Tota, Phys. Rev. Lett. **91**, 064302 (2003).
[7] J. D. Anderson, Phys. Today **58**(12), 42 (2005).
[8] D. Chehata, R. Zenit, and C. R. Wassgren, Phys. Fluids **15**, 1622 (2003).
[9] R. Soller and S. A. Koehler, Phys. Rev. E **74**, 021305 (2006).
[10] Y. Ding, N. Gravish, and D. I. Goldman, Phys. Rev. Lett. **106**, 028001 (2011).
[11] H. Guo, J. Goldsmith, I. Delacruz, M. Tao, Y. Luo, and S. A. Koehler, J. Stat. Mech. (2012) P07013.
[12] A. N. Schofield and P. Wroth, *Critical State Soil Mechanics* (McGraw-Hill, New York, 1968) .
[13] N. Gravish, P. B. Umbanhowar, and D. I. Goldman, Phys. Rev. Lett. **105**, 128301 (2010).
[14] See Supplemental Material at http://link.aps.org/supplemental/10.1103/PhysRevE.88.030201 for (a) a sensitivity analysis of the semiempirical model, (b) the drag on an isosceles triangle intruder, and (c) a comparison of the semiempirical model with the boundary layer approach.
[15] The dimensionless stress components are $\tilde{\sigma}_n = 2.1 + 2.8\cos(\phi) + 0.79\cos(2\phi) - 0.22\cos(3\phi) - 0.23\cos(4\phi)$ and $\tilde{\sigma}_t = 0.25\sin(\phi) + 0.2\sin(2\phi) + 0.055\sin(3\phi) - 0.015\sin(4\phi) - 0.018\sin(5\phi)$.